Article

Structures, Rugged Energetic Landscapes, and Nanothermodynamics of Al (2 ≤ *n* ≤ 65) Particles

Zhen Hua Li, Ahren W. Jasper, and Donald G. Truhlar

J. Am. Chem. Soc., **2007**, 129 (48), 14899-14910 • DOI: 10.1021/ja073129i

J|A|C|S
ARTICLES
Published on Web 11/10/2007

Structures, Rugged Energetic Landscapes, and Nanothermodynamics of Al_n ($2 \leq n \leq 65$) Particles

Zhen Hua Li, Ahren W. Jasper, and Donald G. Truhlar*

Contribution from the Department of Chemistry and Supercomputing Institute, University of Minnesota, Minneapolis, Minnesota 55455-0431

Received May 3, 2007; E-mail: truhlar@umn.edu

Abstract: Metal nanoparticles are important in several emerging technologies, but their size-selected thermodynamic properties are hard to obtain from experiment. We have characterized the energetic and structural properties of unsupported neutral Al_n ($2 \leq n \leq 65$) particles (clusters and nanoparticles) via molecular dynamics quenching simulations with a recently validated many-body analytic potential. For each particle size (n), the global minimum-energy structure, the distribution of the local energy minima, and the finite-temperature thermodynamics have been calculated, the latter by evaluating ~100 000 rovibrational partition functions for the low-energy isomers of the various particles. This analysis demonstrates that the dominant structures of clusters and nanoparticles depend on temperature as well as particle size and that one must consider statistical mechanics as well as electronic structure in determining the dominant structures, stabilities, and properties of nanoparticles. As a particularly dramatic example, although the electronic magic numbers of Al_n are $n = 13$, 19, 23, 38, and 55 when thermal energy is neglected, the $n = 38$ magic number is found to become unstable relative to its neighbors ($n = 37$ and 39) at temperatures of 500 K and above due to vibrational energy and entropy effects. Furthermore, an energy-landscape analysis based on the probability of finding an isomer demonstrates that for many particle sizes, the global-minimum-energy structure on the potential energy surface is not the dominant structure at moderate temperatures, and other low-energy isomers may be dominant at temperatures as low as room temperature. For example, the four lowest-energy structures account for less than 50% of the population for $n = 17$, 31, 33, 34, 36, 37, 39, 41−43, 50, 56, 58, and 63−65 at 300 K and for $n = 10$, 11, and 17−65 at 1500 K. At 1500 K, even the 64 lowest-energy structures account for less than half the population for $n = 23$, 27−55, and 57−65. The increased importance of higher-energy structures at finite temperatures has important implications for understanding the size-selective reactivity and catalytic activity of metal nanoparticles. The isomeric energy (E_{lso}), which is the difference between the thermal average energy of the particle and that of the corresponding global minimum structure in the ground electronic state, is introduced as an indicator of how well the thermochemical properties of a multi-isomer particle can be represented by those of the global minimum structure. Particularly low values for Al_{12}, Al_{13}, Al_{19}, Al_{48}, Al_{53}, Al_{54}, and Al_{56} have been found in a wide temperature range.

1. Introduction

Clusters and nanoparticles have properties distinctly different from those of bulk materials,[1−5] and the possibility of exploiting these unique properties, especially in metallic nanoparticles,[2−4] has inspired intensive experimental and theoretical efforts. One step toward understanding size-dependent phenomena is the characterization of energetically favorable structures as a function of particle size and, in particular, the determination of the most favorable zero-kinetic-energy structures, that is, the global minimum-energy structures. Even for nanoparticles of moderate size, the determination of the global minimum is often not straightforward due to the ruggedness and high dimensionality of the potential energy surface. Many robust searching strategies have been suggested, such as genetic algorithms (SPGA),[6] the basin hopping (BH) method,[7] the big-bang (BB) searching algorithm,[8] and simulated annealing.[9]

The global minimum of a potential energy surface is one of its critical characteristics, but a full understanding of the landscape requires further characterization.[10] We therefore search not only for the lowest-energy structures for each n but also to find a good approximation to the full distribution of all low-energy structures. Thus we can ask: How rugged and multi-

(1) Bernstein, E. R. *Chemical Reactions in Clusters*; Oxford University Press: New York, 1996.
(2) Feldheim, D. L.; Foss, C. A. *Metal Nanoparticles: Synthesis, Characterization, and Applications*; Marcel Dekker: New York, 2002.
(3) Buchachenko, A. L. *Russian Chem. Rev.* **2003**, *72*, 375.
(4) Schmid, G. *Nanoparticles: From Theory to Applications*; Wiley-VCH: Weinheim, 2004.
(5) Baletto, F.; Ferrando, R. *Rev. Mod. Phys.* **2005**, *77*, 371.
(6) Deaven, D. M.; Ho, K. M. *Phys. Rev. Lett.* **1995**, *75*, 288. Ho, K.-M.; Shvartsburg, A. A.; Pan, B.; Lu, Z.-Y.; Wang, C. Z.; Wacker, J. G.; Fye, J. L.; Jarrold, M. F. *Nature* **1998**, *392*, 582. Rata, I.; Shvartsburg, A. A.; Horoi, M.; Frauenheim, Th.; Siu, K. W. M.; Jackson, K. A. *Phys. Rev. Lett.* **2000**, *85*, 546.
(7) Wales, D. J.; Scheraga, H. A. *Science*, **1999**, *285*, 1368; Wales, D. J.; Doye, J. P. K. *J. Phys. Chem. A* **1997**, *101*, 5111.
(8) Jackson, K. A.; Horoi, M.; Chaudhuri, I.; Frauenheim, T.; Shvartsburg, A. A. *Comput. Mater. Sci.* **2006**, *35*, 232.
(9) Kirkpatrick, S.; Gelatt, C. D., Jr.; Vecchi, M. P. *Science* **1983**, *220*, 671.
(10) Wales, D. J. *Energy Landscapes with Applications to Clusters, Biomolecules, and Glasses*; Cambridge University Press: Cambridge, 2003.

peaked are the landscapes? We can also ask: In a thermal distribution, is the particle likely to be found in the vicinity of one or a few deep local minima or must one consider vibrational basins around several or many local equilibrium structures in order to understand the properties of metal nanoparticles? Understanding the answers to these questions is a prerequisite to the rational design of functional nanoparticles, but the answers are difficult to obtain experimentally because it is not easy to obtain a monodisperse size distribution although some methods do exist[11,12] and it is even harder to characterize the ruggedness of the energy landscapes of clusters and nanoparticles. Thus, the simulations presented here yield information that is hard to obtain by other techniques, either analytical (pure theory) or experimental.

Although the characterization of the global and local minima as a function of cluster size is useful in understanding relative reactivities, catalytic efficiencies, and particle growth, such studies neglect the important roles of zero-point energy, thermal energy, and entropy. Even at moderate temperatures, fluctuations away from the minima may have important implications for the properties of thermal systems. These fluctuations can best be understood by calculating free energies, which requires entropic as well as energetic considerations. The key to extending thermodynamics to small systems,[13] that is, generalizing macrothermodynamics to nanothermodynamics,[14] is the introduction of the ensemble-average energy as a function of particle size.[15] Whereas macroscopic systems typically have negligible fluctuations in energy, small systems, such as nanoparticles, have large fluctuations relative to their average energy. In the present article, an analysis of the importance of these fluctuations in understanding the relative stability of Al nanoparticles is presented. In particular, the present article takes up this task for Al_n molecules (also called particles) with n in the range 2−65, where molecules with $n \leq 19$ are called clusters, and those with $n \geq 20$ are called nanoparticles. The boundary between clusters and nanoparticles is somewhat arbitrary but corresponds to a diameter of ∼1 nm. Al clusters and nanoparticles are studied from 300 K (where the particles are nanocrystallites) to 1500 K (where they are nanodroplets, which would be their physical state in most chemical vapor depositions and plasma environments). The calculation of the isomer distribution in an ensemble of nanoparticles is very challenging because of the rugged landscape with multiple, diverse metastable states, but it is essential to provide a foundation for extending statistical thermodynamic characterization techniques into the nano regime where fluctuations are commensurate with mean values.[10,13−21]

The existence of a multitude of low-energy isomers in metal nanoparticles has implications for their use as chemical catalysts, both because of the possibility for making more adsorption sites available and also because of the possibility of adsorbate-induced structural change.[22]

The present analysis also has important implications for understanding phase transitions in nanoparticles.[5,7,23,24] The melting or freezing of a nanoparticle involves a phase transition or structural transition from a solid-like structure to a liquid-like structure (melting) or vice versa (freezing), and structural as well as thermochemical properties are often used to characterize these transitions. Knowledge of the distribution of low-lying metastable configurations as well as their contribution to the thermodynamics of the particle as a function of temperature and particle size is required for a better understanding of this phenomenon.

The physical and chemical properties of Al particles have been studied theoretically,[25−30] often by using analytic potentials.[31−34] These potentials, however, are usually obtained by fitting to the bulk aluminum properties and are inaccurate for the energetics of the clusters and nanoparticles.[35] Recently, economical and accurate analytical potentials for aluminum systems have been developed by fitting to highly accurate electronic-structure data for Al_n clusters and nanoparticles as well as experimental bulk properties.[35,36] These analytic potentials allow for efficient and extensive searches of the potential energy landscapes of aluminum nanoparticles, whereas the use of first principle methods is feasible only for selected small clusters.[37−39]

In this paper, we first present a method; for searching for global minima of clusters and nanoparticles, then we apply it to Al_n particles (clusters and nanoparticles) with $n = 2-65$ using the NP−B potential energy function[36] for the ground electronic state that was previously validated for pure Al clusters and nanoparticles using a large and diverse dataset of density functional theory (DFT) structures and energies;[36] the DFT method was itself validated for the smallest clusters by comparison to wave function theory and experiment.[40] The NP−B potential assumes that the electronic energy is separable and that the average electronic excitation energy is independent

(11) Buck, U.; Krohne, R. *J. Chem. Phys.* **1996**, *105*, 5408.
(12) Wöste, L. *Z. Phys. Chem.* **1996**, *196*, 1. Murray, C. B.; Sun, S.; Doyle, H.; Betley, T. *MRS Bull.* **2001**, *26*, 985. Kim, J. H.; Germer, T. A.; Mulholland, G. W.; Ehrman, S. H. *Adv. Mater* **2002**, *14*, 518. Chandra, A.; Clemens, B. M. *J. Appl. Phys.* **2004**, *96*, 6776. Kohno, M.; Orii, T.; Hirasawa, M.; Seto, T.; Murakami, Y.; Chiashi, S.; Miyauchi, Y.; Maruyama, S. *Appl. Phys. A: Mater. Sci. Process.* **2004**, *79*, 787. Qu, L.; Dai, L.; Osawa, E. *J. Am. Chem. Soc.* **2006**, *128*, 5523. Yu, S.; Sun, C.-J.; Chow, G.-M. In *Nanostructured Materials*, 2nd ed.; Koch, C. C., Ed.; William Andrew Publishing: Norwich, NY, 2007; p 3.
(13) Hill, T. L. *J. Chem. Phys.* **1962**, *36*, 3182. Hill, T. L. *Thermodynamics of Small Systems*; Dover: New York, 1994. Hill, T. L. *Nano Lett.* **2001**, *1*, 111. Hill, T. L. *Nano Lett.* **2001**, *1*, 273.
(14) Hill, T. L.; Chamberlin, R. V. *Proc. Natl. Acad. Sci. U.S.A.* **1998**, *95*, 12779. Chamberlin, R. V. *Nature* **2000**, *408*, 337. Giebultowicz, T. *Nature* **2000**, *408*, 299.
(15) Debenedetti, P. G.; Stillinger, F. H.; Truskett, T. M.; Roberts, C. J. *J. Phys. Chem. B* **1999**, *103*, 7390.
(16) Jellinek, J.; Goldberg, A. *J. Chem. Phys.* **2000**, *113*, 2570.
(17) Nave, E. L.; Mossa, S.; Sciortino, F. *Phys. Rev. Lett.* **2002**, *88*, 225701.
(18) Apol, M. E. F.; Amadei, A. *J. Phys. Chem. B* **2003**, *107*, 1410.
(19) Wales, D. J.; Doye, J. P. K. *J. Chem. Phys.* **2003**, *119*, 12409.
(20) Keyes, T.; Chowdhary, J. *Phys. Rev. E* **2004**, *69*, 41104.
(21) Attili, A.; Gallo, P.; Rovere, M. *Phys. Rev. E* **2005**, *71*, 31204.
(22) Gu, X.; Bulusu, S.; Li, X.; Zeng, X. C.; Li, J.; Gong, X. C.; Wang, L.-S. *J. Phys. Chem. C* **2007**, *111*, 8228.
(23) Berry, R. S. In *Microscale Energy Transport*; Tien, C. L., Majumdar, A. C., Gerner, F. M., Eds.; Taylor & Francis: Washington, 1998; p 149. Proykova, A.; Radev, R.; Li, F.-Y.; Berry, R. S. *J. Chem. Phys.* **1999**, *110*, 3887. Proykova, A.; Berry, R. S. *J. Phys. B* **2006**, *39*, R167.
(24) Alonso, J. A. *Structure and Properties of Atomic Nanoclusters*; Imperial College Press: London, 2005.
(25) Cheng, H.-P.; Berry, R. S.; Whetten, R. L. *Phys. Rev. B* **1991**, *43*, 10647.
(26) Elbayyariz, Z.; Erkoc, S. *Phys. Status Solidi B* **1992**, *170*, 103.
(27) Lloyd, L. D.; Johnston, R. L. *Chem. Phys.* **1998**, *236*, 107.
(28) Turner, G. W.; Johnston, R. L.; Wilson, N. T. *J. Chem. Phys.* **2000**, *112*, 4773.
(29) Joswig, J.-O.; Springborg, M. *Phys. Rev. B* **2003**, *68*, 085408.
(30) Sebetci, A.; Güvenç, Z. B. *Modell. Simul. Mater. Sci. Eng.* **2005**, *13*, 683.
(31) Voter, A. F.; Chen, S. P. *Mater. Res. Soc. Symp. Proc.* **1987**, *82*, 175.
(32) Murrell, J. N.; Mottram, R. E. *Mol. Phys.* **1990**, *69*, 571. Murrell, J. N.; Rodriguez-Ruiz, J. *Mol. Phys.* **1990**, *71*, 823.
(33) Sutton, A. P.; Chen, J. *Philos. Mag. Lett.* **1990**, *61*, 139.
(34) Cleri, F.; Rosato, V. *Phys. Rev. B* **1993**, *48*, 22.
(35) Jasper, A. W.; Staszewski, P.; Staszewski, G.; Schultz, N. E.; Truhlar, D. G. *J. Phys. Chem. B* **2004**, *108*, 8996.
(36) Jasper, A. W.; Schultz, N. E.; Truhlar, D. G. *J. Phys. Chem. B* **2005**, *109*, 3915.
(37) Jones, R. O. *Phys. Rev. Lett.* **1991**, *67*, 224. Jones, R. O. *J. Chem. Phys.* **1993**, *99*, 1194.
(38) Ahlrichs, R.; Elliott, S. D. *Phys. Chem. Chem. Phys.* **1999**, *1*, 13.
(39) Rao, B. K.; Jena, P. *J. Chem. Phys.* **1999**, *111*, 1890.
(40) Schultz, N. E.; G. Staszewska, P. Staszewski, Truhlar, D. G. *J. Phys. Chem. B* **2004**, *108*, 4850.

of cluster size as well as isomer, but it does not assume that the ground electronic state is a singlet or a doublet. In developing the potential, the spin states of the clusters and nanoparticles have been taken into consideration in calculating the ground-state energy, and if a triplet state or quartet state (for example) is the ground state, the energy used for fitting the potential is the energy of that state. Although considering just the ground electronic state is an approximation, the cohesive energy extrapolated to the bulk limit is just 0.02 eV higher than the experimental value (an error of only 0.6%). The NP−B potential used here has been applied to the critical point and phase behavior of elemental aluminum and the results are promising and agree with available experimental results.[41,42]

Section 2 presents the simulation methods. The searching algorithm is a combination of the big-bang searching algorithm and a method similar to the conventional simulated annealing algorithm. Section 3 discusses the low-energy structures predicted for the NP−B force field. On the basis of finding and characterizing an ensemble of structures, we discuss the energy landscapes and thermochemical properties of the Al_n clusters and nanoparticles in Section 4. Important points made in that section include the importance of vibrational free energy (i.e., structures other than local minima of the potential energy surface) and the importance of isomeric free energy (i.e., the importance of basins other than the one associated with the global lowest-energy structure). Section 5 summarizes some of the conclusions.

2. Simulations

Full details of the simulations are provided in Supporting Information. Here we simply summarize them.

Big-Bang (BB) Searching Algorithm. For each particle size n, 10 000 highly compressed nearly spherical particles were randomly generated. Each of the randomly generated clusters was then optimized to the nearest local minimum. The lowest-energy structure in the resulting distribution of local minima for each n is denoted the big-bang global minimum (BBGM).

Many of the local minima that are found correspond to the same structure, and energetic and geometric criteria were used to determine the final set of distinct local minima.

Molecular Dynamics Simulation and Quenching (MDSQ) Method. Molecular dynamics (MD) simulations were also performed for each cluster size n. Ten independent low-energy trajectories were started from the BBGM; their temperatures were slowly raised to 1000 K for $n > 30$ and to 1400 K for $n \le 30$; these temperatures are several hundred degrees above the melting points, which are ~600−700 K for the large-sized nanoparticles[43] and ~1100 K for a cluster as small as Al_{13}.[44] (For comparison, the bulk melting point of Al is 933 K.[45]) During the MD simulations, randomly selected configurations were quenched to the nearest local minimum. For nanoparticles for $n > 30$, an average of 246 000 configurations were quenched, while for the smaller clusters, an average of 366 000 were quenched. A set of up to 2000 distinct local minima was obtained from the quenched structures by again using energetic and geometric criteria.

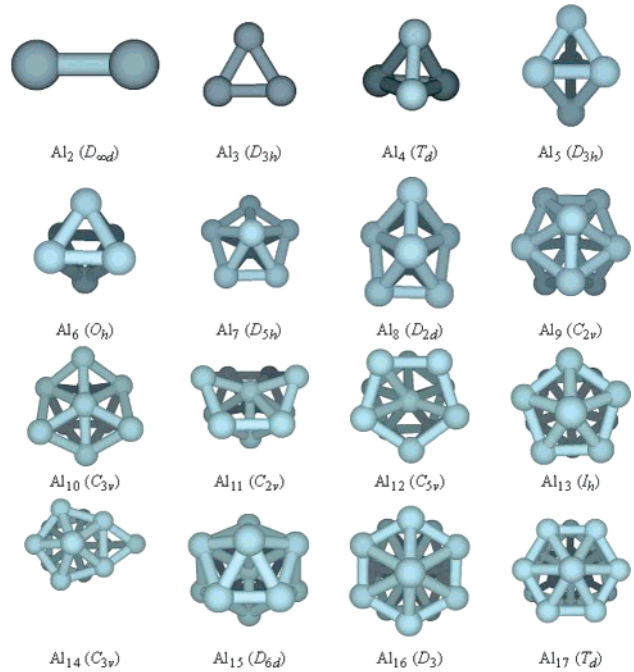

Figure 1. Structures and symmetries of the global minima with $n = 2-17$ located by the combination of the BB and MDSQ methods.

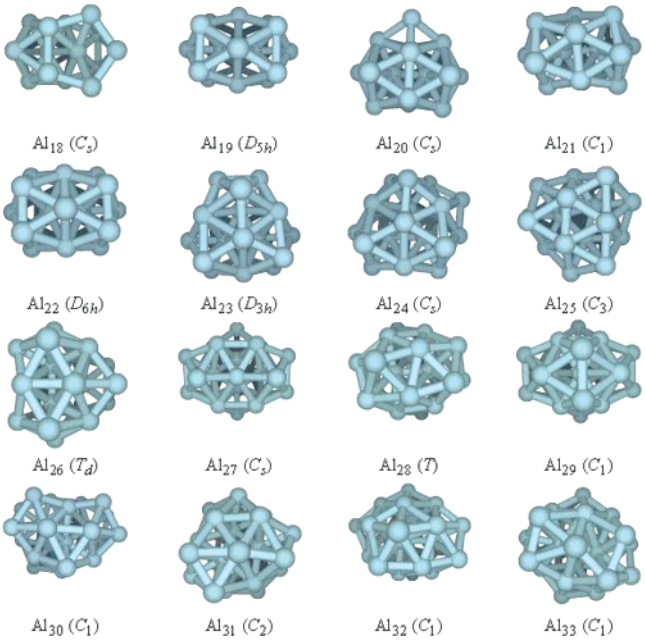

Figure 2. Structures and symmetries of the global minima with $n = 18-33$ located by the combination of the BB and MDSQ methods.

3. Structures

The distinct minima found by the two searching methods are in generally good agreement, and this validates the collection of structures for use in further analysis. These distinct structures will henceforth be called isomers. The lowest-energy isomers (also called the global minima) for $n = 2-65$ are illustrated in Figures 1−4. The second-, third-, and fourth-lowest-energy isomers for Al_4-Al_9 and Al_{61} are illustrated in Figure 5.

(41) Bhatt, D.; Jasper, A. W.; Schultz, N. E.; Siepmann, J. I.; Truhlar, D. G. *J. Am. Chem. Soc.* **2006**, *128*, 4224.
(42) Bhatt, D.; Schultz, N. E.; Jasper, A. W.; Siepmann, J. I.; Truhlar, D. G. *J. Phys. Chem. B* **2006**, *110*, 26135.
(43) Breaux, G. A.; Neal, C. M.; Cao, B.; Jarrold, M. F. *Phys. Rev. Lett.* **2005**, *94*, 173401.
(44) Akola, J.; Manninen, M. *Phys. Rev. B* **2001**, *63*, 193410.
(45) Chase, M. W., Jr. *NIST-JANAF Thermochemical Tables*, 4th ed.; J. Phys. Chem. Ref. Data Monograph Series No. 9; American Institute of Physics: New York, 1998.

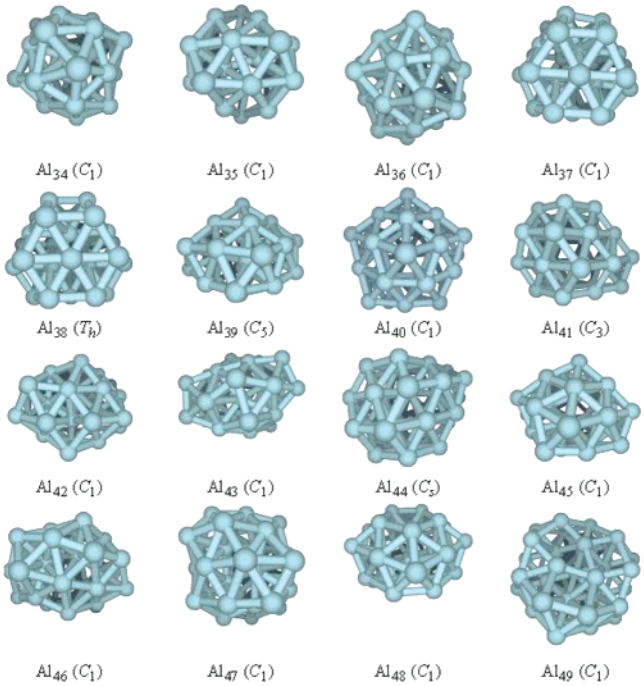

Figure 3. Structures and symmetries of the global minima with $n = 34-49$ located by the combination of the BB and MDSQ methods.

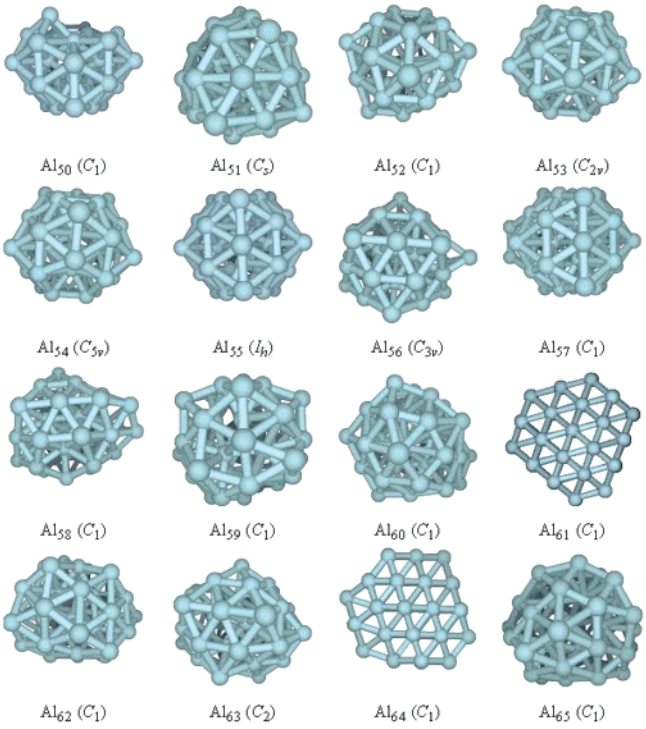

Figure 4. Structures and symmetries of the global minima with $n = 50-65$ located by the combination of the BB and MDSQ methods.

For Al_7, the present simulations predict a D_{5h} structure as the global minimum. The capped octahedral structure with C_{3v} symmetry predicted[37,38] by DFT as the global minimum is the second-lowest-energy isomer with NP−B and is higher in energy by 0.17 eV. The global minimum of Al_8 predicted here has D_{2d} symmetry, which can be viewed as an octahedron with two Al atoms capping two adjacent faces. The second-lowest-energy isomer is a structure that can be described as $D_{5h}-Al_7$ with a cap on one of the faces. An isomer with D_{3d} symmetry,

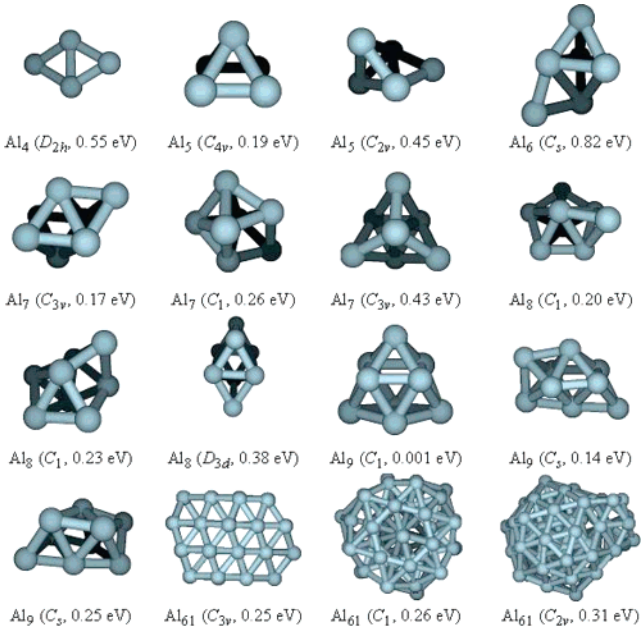

Figure 5. Structures of the second-, third-, and fourth-lowest-energy isomers (note that for Al_4-Al_6 less than four isomers were found), if available, of Al_4-Al_9 and Al_{61} located by the combination of the BB and MDSQ methods. Values in the parentheses are the symmetries and energies ΔE relative to the global minima.

which distorts to the D_{2h} global minimum predicted by Jones[37] and Ahlrichs and Elliott[38] using DFT methods, is the fourth-lowest-energy isomer, higher in energy by 0.38 eV.

The global minima for Al_9-Al_{13} may be understood as being grown from $D_{5h}-Al_7$: Al_9 is $D_{5h}-Al_7$ capped with two Al atoms on the two adjacent faces on the same side of the symmetry plane perpendicular to the C_5 axis; Al_{10} is $D_{5h}-Al_7$ capped by three adatoms, and so on. The icosahedral Al_{13} can be viewed as two $D_{5h}-Al_7$ sharing one vertex Al atom. For Al_9, the BB and MDSQ searches found an isomer (Figure 5, Al_9 (C_1)) almost degenerate with (only 0.006 eV higher than) the global minimum. Further high-level calculations are needed to confirm the stability of this low-energy isomer.

Al_{19} is the largest cluster for which the global minimum has been characterized using a DFT potential and simulated annealing searches.[38] For the clusters in this range, the predicted global minima are in general agreement with previous results,[25−30,46] with one important exception. Analytical potentials tend to prefer structures with higher symmetry, which would distort to lower-symmetries if Jahn−Teller electronic effects were included.[37−39]

For particles smaller than Al_{13}, all the atoms in the cluster are surface atoms. For $n = 13-18$, the global minima have shell structures with one interior atom. The global minima of $Al_{19}-Al_{22}$ have two interior atoms. From Al_{23} onward, the global minima have at least 3 interior atoms For $n > 19$, the global minima generally agree well with structures predicted by other analytical potentials using other algorithms when such results[27,29,30] are available. In particular, the global minimum of Al_{38} is a truncated octahedron, and that of Al_{55} is an icosahedron.

Although the potential used here has been well validated for Al_n nanoparticles, it does not account fully for the very specific

(46) Chuang, F.-C.; Wang, C. Z.; Ho, K. H. *Phys. Rev. B* **2006**, *73*, 125431.

properties of the smallest particles. For example, although the most accurate calculations[37,38,40,47] indicate that the global minima for both Al_4 and Al_5 are planar, with NP−B the planar Al_4 and Al_5 are higher in energy than the global minima (tetrahedral for Al_4 and trigonal bipyramidal for Al_5[36]) 0.55 and 1.07 eV, respectively (other empirical potentials show similar discrepancies for very small n[27,29,30]). A recent parametrization of tight-binding theory predicts a planar global minimum for Al_4,[48] which agrees with higher-level calculations,[37−40,48] but the same tight binding potential fails to predict a planar global minimum-energy structure for Al_5.[48] The planar structure of Al_5 was not located in the BB or MDSQ searches with NP−B because it is a saddle point. However, the Al_5 search located a structure with C_{2v} symmetry that may be obtained by adding an atom to one edge of the Al_4 tetrahedron. The stability of the structure was verified using DFT calculations with the PBE0[49] functional and the MG3 basis set,[50] and this structure was found to be higher in energy than the PBE0 global minimum (the planar C_{2v} structure) by only 0.32 eV. This structure was seldom studied in previous discussion of Al_n structures except one.[51] For Al_6, the global minimum predicted by the analytic potential is an octahedron (O_h symmetry). Density functional theory (DFT)[37,38] and ab initio QCISD[40] calculations indicate that the global minimum of Al_6 is a D_{3d} structure Jahn−Teller distorted away from the octahedral structure. The low-energy prism structure reported by Ahlrichs and Elliott[38] was not located in the current work. These quantitative issues for small clusters do not prevent us from drawing interesting conclusions in the present study because the NP−B potential is accurate enough for nanoparticles ($n \gtrsim 19$) to study the questions of energy landscapes that form the unique focus of the present study.

4. Energy Landscapes

Global Minima. The cohesive energy, CE(n), of the particle of size n is defined as

$$\mathrm{CE}(n) = E_e(1) - E_e^{(1)}(n)/n \qquad (1)$$

where $E_e^{(\gamma)}(n)$ is the potential energy of the classical-equilibrium structure of the isomer γ of the particle of size n, and we have set $\gamma = 1$ on the right-hand side of eq 1 to denote the global minimum (γ is not needed for $n = 1$). Note that the potential energy for nuclear motion that appears in this definition is the Born−Oppenheimer electronic energy of the ground electronic state of the system, including nuclear repulsion. Following the spectroscopic convention, the subscript "e" denotes a classical-equilibrium value,[52] that is, that thermal and zero-point vibrational energy (ZPE) contributions are excluded.

The experimental bulk cohesive energy is 3.43 eV,[53] exclusive of zero-point vibrational contributions, as discussed in ref 40. The CEs for the Al_n particles are plotted as a function of n in Figure 6. For $n \ge 13$, the expression (see Figure S2 in Supporting Information for a plot)

$$\mathrm{CE}(n) = E_{coh} - Bn^{-1/3} \qquad (2)$$

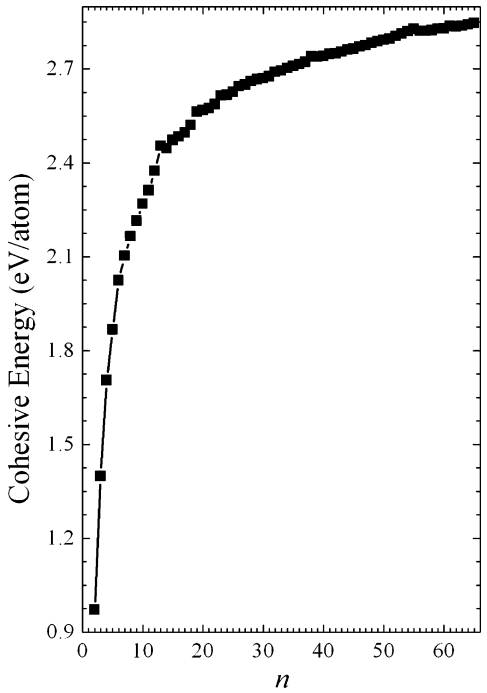

Figure 6. Cohesive energies of the global minima as a function of n for $n = 2-65$. A table of these values is included in Supporting Information as Table S1.

predicts an extrapolated bulk cohesive energy E_{coh} of 3.45 eV/atom, which is only 0.02 eV higher than the experimental value.

Probabilities of the Isomers. A key issue in nanoparticle science is the importance of low-energy isomers for the average properties of the particles. This subject has often been neglected because, at least for realistic potentials, usually only the properties of the global minimum are studied. (For exceptions, see ref 10.) Here we will explore this question by considering the classical rovibrational partition functions (q_{Rov}) of the sets of isomers found by the searches.

For molecules with a single structure (i.e., a single isomer), one may approximate the internal partition function as a product of electronic, vibrational, and rotational partition functions, which is equivalent to assuming that q_{Rov} is independent of electronic state and the rotational partition function (q_{Rot}) is independent of the electronic and vibrational states. This is called the separable approximation.[53−56] Similarly for a molecule with more than one isomer, one can make a separable approximation that the electronic partition function (q_{Elec}) is the same for all the isomers. Then the internal partition function of a particle is approximated as

$$Q = q_{Elec} \sum_{\gamma} [e^{-E_e^{(\gamma)}/kT} \sum_{v,j} e^{-\epsilon_{\gamma,v,j}/kT}] \qquad (3)$$

where $\epsilon_{\gamma,v,j}$ is the ground-electronic-state rovibrational energy level of isomer γ relative to the local minimum $E_e^{(\gamma)}$ of the isomer; v and j denote the collections of vibrational and

(47) Petterson, L. G. M.; Bauschlicher, C. W., Jr.; Halicioglu, T. *J. Chem. Phys.* **1987**, *87*, 2205.
(48) Jasper, A. W.; Schultz, N. E.; Truhlar, D. G. *J. Chem. Theory Comput.* **2007**, *3*, 210.
(49) Adamo, C.; Barone, V. *J. Chem. Phys.* **1999**, *110*, 6158.
(50) Lynch, B. J.; Zhao, Y.; Truhlar, D. G. *J. Phys. Chem. A* **2003**, *107*, 1384.
(51) Chi, X.; Xi, S.; Zhuang, Y.; Xu, K. *Chin. J. Chem. Phys.* **2002**, *15*, 269.
(52) Herzberg, G. *Electronic Spectra of Polyatomic Molecules*; Van Nostrand Reinhold: New York, 1966; p 20.
(53) Brewer, L. *The Cohesive Energy of the Elements. Report 3720*; Lawrence Berkeley Laboratory: Berkeley, CA, 1973.
(54) Hill, T. L. *An Introduction to Statistical Thermodynamics*; Addison-Wesley: Reading, MA, 1960; p 149.
(55) McQuarrie, D. A. *Statistical Mechanics*; Harper & Row: New York, 1975; p 130.
(56) Berry, R. S.; Rice, S. A.; Ross, J. *Physical Chemistry*, 2nd ed.; Oxford University Press: New York, 2000; p 570.

rotational quantum number, respectively, k is the Boltzman constant, and T is temperature. The sum over rovibrational energy levels yields the rovibrational partition function of an isomer,

$$q_{\mathrm{Rov}}^{(\gamma)} = \sum_{v,j} e^{-\epsilon_{\gamma,v,j}/kT} \tag{4}$$

To calculate $q_{\mathrm{Rov}}^{(\gamma)}$, we assume that $q_{\mathrm{Rov}}^{(\gamma)}$ is the product of $q_{\mathrm{Rot}}^{(\gamma)}$ and vibrational partition function ($q_{\mathrm{Vib}}^{(\gamma)}$). The former is calculated classically using the rigid-rotor approximation, and the latter is calculated using the harmonic-oscillator approximation (HOA) for high-frequency modes and an effective HOA for low-frequency modes (see Supporting Information).

By assuming that all the isomers are populated according to an equilibrium distribution, the probability of one particular isomer of Al_n can be estimated by

$$P_\gamma = \frac{e^{-E_{\mathrm{e}}^{(\gamma)}/kT} q_{\mathrm{Rov}}^{(\gamma)}}{\sum_\gamma e^{-E_{\mathrm{e}}^{(\gamma)}/kT} q_{\mathrm{Rov}}^{(\gamma)}} \tag{5}$$

where P_γ, $E_{\mathrm{e}}^{(\gamma)}$, and $q_{\mathrm{Rov}}^{(\gamma)}$ all refer to a specific n. Our most accurate results are based on eq 5. P_γ calculated without considering $q_{\mathrm{Rot}}^{(\gamma)}$, or in another perspective, by assuming that all isomers have the same q_{Rot} as the global minimum, has been used by other researchers to analyze the size-dependence of the properties of Lennard-Jones (LJ) clusters,[57] strontium clusters,[58,59] copper and silver clusters,[60] and Ag−Ni and Ag−Cu clusters and nanoparticles.[61]

For comparison, the further assumption could be made that $q_{\mathrm{Rov}}^{(\gamma)}$ is independent of the isomer structure, that is, that it equals $q_{\mathrm{Rov}}^{(1)}$ for all γ. The probability is then estimated by

$$P_\gamma^{\mathrm{IS}} = \frac{e^{-E_{\mathrm{e}}^{(\gamma)}/kT}}{\sum_\gamma e^{-E_{\mathrm{e}}^{(\gamma)}/kT}} \tag{6}$$

Here we name this approximation the isomerically separable (IS) approximation. To distinguish eq 5 from this IS method, we will call it isomerically coupled (IC) or, for short, nonseparable. It is important to emphasize the physical difference. The isomerically separable method ignores the differences in entropy, thermal energy, and zero-point vibrational energy between the various isomers, whereas the coupled calculation includes these effects. More informally, one can say that the separable method addresses the isomeric distribution entirely in terms of the properties of optimized structures, whereas the coupled approach adds statistical mechanics.

Distribution of Energy-Minimum Structures. The probabilities of the first- through fourth-lowest-energy isomers calculated by the coupled and separable methods are given in the Supporting Information. However, the trends are clearer when one examines the cumulative probabilities defined by

$$C_N = \sum_{\gamma=1}^{N} P_\gamma \tag{7}$$

(Note that $C_1 = P_1$.) Cumulative probabilities for $N = 1$, 2, 4, 8, 16, 32, and 64 are shown in Figure 7 at 300 and 1500 K.

Distributions calculated using the separable approximation show several qualitative differences from those calculated nonseparably, even at 300 K. For most particles at room temperature, the IS approximation predicts that the global minimum always has a probability higher than 50%, although there are also several particles, for example $n = 9$ and 64, for which the second-lowest-energy isomers have probabilities comparable to that of the global minimum. For some particles, for example, $n = 16$, 22, 39, 57, and 58, even the third-lowest-energy isomers have probabilities greater than 10%. However, using the less approximate coupled method, the second-lowest-energy isomer becomes the dominant structure for some particles, for example, for $n = 9$, 22, 32, and 39. For $n = 9$ and 32, the probability of the second-lowest-energy isomer is even higher than 50%. For $n = 61$, the third-lowest-energy isomer becomes the dominant structure, with a probability higher than 90%.

At 1500 K, above the particle melting points, the only particles for which the global minimum dominates ($P_1 > 50\%$) are $n = 2-6$ and 13, all smaller than the smallest nanoparticle ($n \approx 20$). Furthermore, only 14 particle sizes, $n = 2-6$, 8−10, 12−14, 16, 19, and 26, have $P_1 > 0.2$. In contrast, the IS approximation predicts that $P_1 > 0.50$ for $n = 2-8$, 12, 13, 19, 23, and 55, and that $P_1 > 0.20$ for 20 particle sizes, $n = 2-10$, 12−15, 19, 23, 26, 38, and 53−55. The particularly high value of P_1^{IS} at $n = 13$, 19, 23, 38, 55, and 61 are due to large energy gaps between the global minimum and the second-lowest-energy isomer, the gaps being 1.01, 0.67, 0.55, 0.45, and 0.70 eV, respectively. However, after accounting for entropy and thermal energy, the P_1 values at $n = 38$, 55, and 61 drop below 0.01. In addition, assuming isomeric separability implies that the global minima always have higher probabilities than other isomers, while nonseparably, that is, including thermal effects and entropy, other low-energy minima have higher probability than global minima at 1500 K, for example the second-lowest-energy isomer for $n = 7$, 8, 9, 15, 22, 29, 32, 38, 39, 42, 43, 50, and 54−58; the third-lowest-energy isomer for $n = 7$, 22, 49, 50, 55−58, and 63; and the fourth-lowest-energy isomer for $n = 32$, 49, 50, and 56−60. These considerations highlight the importance of entropy, thermal energy, and ZPE in determining the isomer distribution.

Analysis of the results in more detail leads to two interesting general observations. Usually higher-energy isomers have lower symmetry than global minima, and thus have smaller symmetry numbers (which appear in the denominator of q_{Rot}) and thus have larger q_{Rot} than the global minima, that is, the phase space associated with disordered clusters is typically much larger than the phase space associated with highly symmetric structures. Furthermore, global minima are usually more closely packed, and thus have fewer small frequencies than higher-energy isomers. Therefore, even for those particles with a large energy gap between the global minimum and other isomers, it is possible that higher-energy isomers have larger probabilities when q_{Rov} is taken into consideration. (In other words, the degree of order and the density of packing are often smaller for higher-energy structures, which may then become the dominant ones

(57) Doye, J. P. K.; Calvo, F. *Phys. Rev. Lett.* **2001**, *86*, 3570.
(58) Wang, G. M.; Blaisten-Barojas, E.; Roitberg, A. E. *J. Chem. Phys.* **2001**, *115*, 3640.
(59) Doye, J. P. K.; Calvo, F. *J. Chem. Phys.* **2003**, *119*, 12680.
(60) Baletto, F.; Rapallo, A.; Rossi, G.; Ferrando, R. *Phys. Rev. B* **2004**, *69*, 235421.
(61) Rossi, G.; Rapallo, A.; Mottet, C.; Fortunelli, A.; Baletto, F.; Ferrando, R. *Phys. Rev. Lett.* **2004**, *93*, 10553.

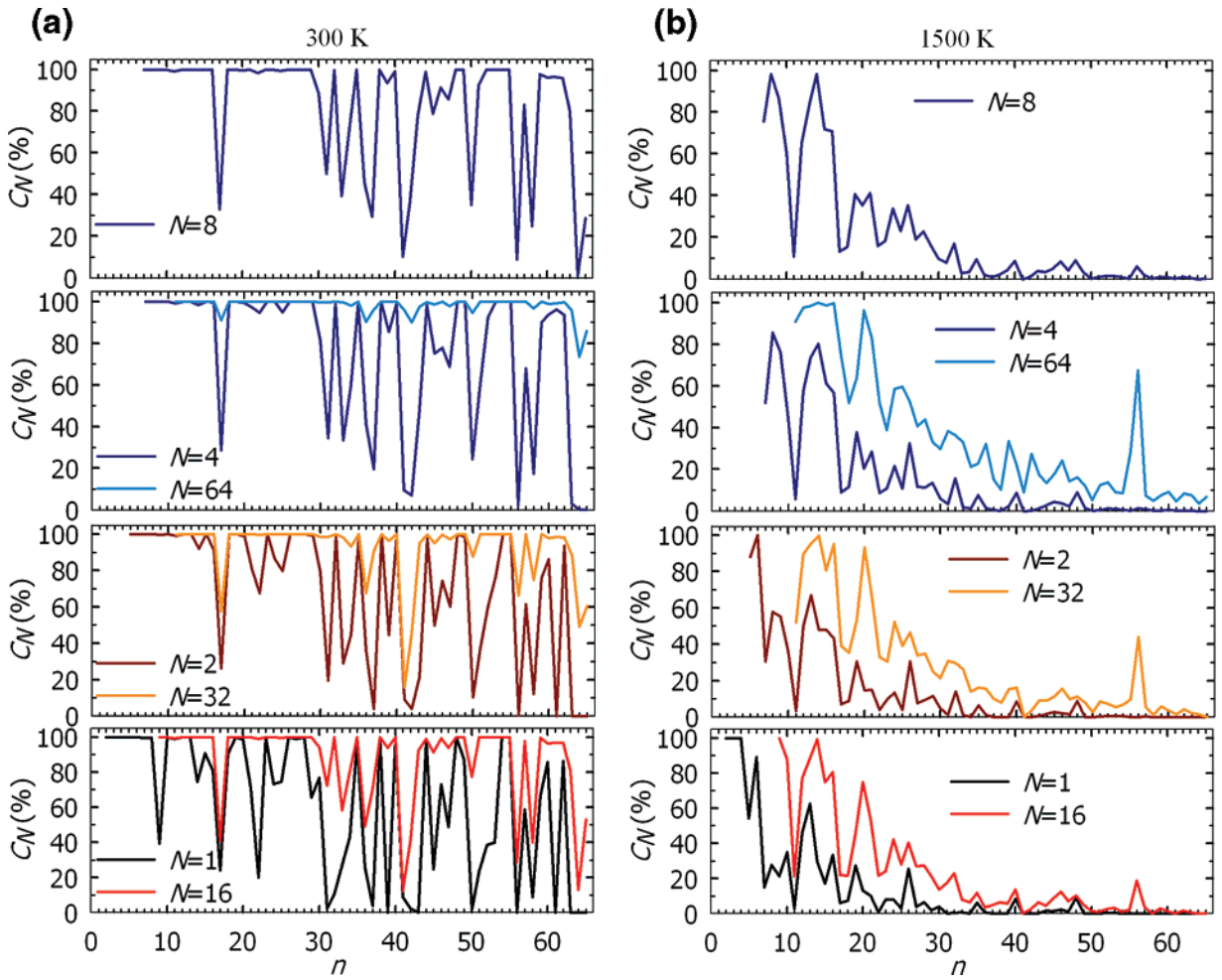

Figure 7. Cumulative probability of the N lowest-energy isomers given by eq 7 as a function of cluster size at (a) 300 K and (b) 1500 K.

at higher temperatures because entropic considerations become more important with increasing temperature.) For the particles with just a few atoms (also called clusters), there are just a few low-energy isomers; even the contributions calculated by the nonseparable method show that for these small clusters the global minimum is dominant even at 1500 K. As the cluster size increases, more and more low-energy isomers appear, and as the temperature rises, their population may increase significantly. For example, for $n = 38$, the global minimum is no longer dominant by 600 K, and the probabilities of the fourth- and sixth-lowest-energy isomers are non-negligible already at 400 K. (Interestingly, Wales[12] found that the global minimum of Ar_{38} is also special, in that case because it lies at the bottom of a narrow side potential energy funnel in a disconnectivity diagram. The pairwise Lennard-Jones potential used in that study is quite different from the many-body potential used here.)

The global minimum has a population below 0.2 at 300 K for $n = 31$, 32, 37, 39, 41−43, 50, 56, 61, and 63−65, and it is 0.24 for $n = 17$ and 51 and 0.20 for $n = 22$. Thus these particle sizes provide the most dramatic example of statistical mechanics trumping conclusions based only on optimized global minima. We will take Al_{61} as a case study to analyze this effect, and to do so we define the vibrational density of states as

$$\rho_{\text{Vib}} = \frac{\mathrm{d}n_\omega}{\mathrm{d}\omega} \tag{8}$$

where n_ω is the number of vibrational states between frequency ω and frequency $\omega + \mathrm{d}\omega$; ρ_{Vib} is obtained by a Legendre moment method.[62]

Figure 8 indicates that the third-lowest-energy isomer of Al_{61} has higher ρ_{Vib} for frequencies below 150 cm^{-1}. The global minimum and the second-lowest-energy minimum have more vibrational states at higher frequencies (above 250 cm^{-1}). As mentioned earlier, the low frequencies make large contributions to the partition functions. In Figure 5 we also depicted the structure of the second-, third-, and fourth-lowest-energy isomers for Al_{61}. One can see that the global minimum (Figure 4) and the second-lowest-energy isomer (Figure 5) both have a face-centered (FCC) close-packed structure, whereas the third-lowest-energy isomer has an irregular structure. This is the reason that the third-lowest-energy isomer has more low-frequency vibrational modes and thus has a higher probability than the global minimum.

The above discussion shows that for many large particles the global minimum has a small probability and thus makes a relatively small contribution to the properties of the particle even at room temperature. This allows us to achieve a greater understanding of the trends in Figure 7. At room temperature (Figure 7a), for the particles with $n < 30$, except for $n = 17$ and 22, the global minimum and the second-lowest-energy isomer contribute most to the properties of particles, with $C_2 > 0.8$. For $n = 17$ and 22, four and more than 32 low-energy

(62) Truhlar, D. G.; Blais, N. C. *J. Chem. Phys.* **1977**, *67*, 1532.

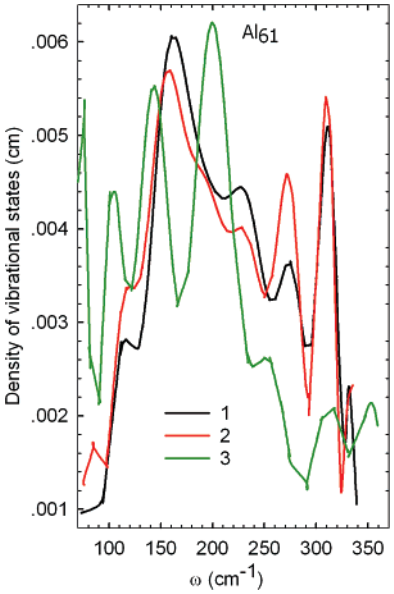

Figure 8. Density of vibrational states of the three lowest-energy isomers of $Al_{61}$with "1" representing the global minimum, "2" the second-lowest-energy isomer, and "3" the third-lowest-energy isomer.

isomers, respectively, make important contributions to the particle properties. However, for *many* particles with $n \geq 30$, more than four isomers need to be considered. For some particles, even the cumulative probability of the 16 lowest-energy isomers is small; this occurs for particles with $n = 41$, 50, 56, and 64. For most particles, it is sufficient to consider the 32 lowest-energy isomers, but for $n = 41$ and 64, even considering the 32 lowest-energy isomers is not enough. At 1500 K (Figure 7b), higher-energy isomers contribute more to the properties of the particles. For most particles with $n > 20$, even the 64 lowest-energy isomers make small contributions (usually less than 50%) at 1500 K.

Cohesive Energy Analysis. The cohesive energies may be used in various ways to characterize the stability of the particles.[4] One parameter characterizing the stability of a particle is its excess energy $\Delta(n)$, which is defined as[5]

$$\Delta(n) = n^{(1/3)}[CE(n) - E_{coh}] \quad (9)$$

Another stability parameter is the second finite difference, $\Delta_2 E_e^{(1)}(n)$, which is the energy released by migrating one Al atom from Al_{n+1} to Al_{n-1} to form two Al_n particles, and it is defined as[5]

$$\Delta_2 E_e^{(1)}(n) = E_e^{(1)}(n-1) + E_e^{(1)}(n+1) - 2E_e^{(1)}(n) \quad (10)$$

Magic Numbers. Figure 9 shows $\Delta(n)$ vs n, and the second finite energy differences are plotted as functions of n in Figure 10. Peaks in the plots correspond to global minima that are stable relative to their neighbors, and valleys correspond to unstable particles. There are five clear peaks in the plot of $\Delta(n)$, and they occur at $n = 13$, 19, 23, 38, and 55. These values of n are also the highest peaks in Figure 10. Thus these are the most probable candidates for the magic numbers based on the usual type of analysis, that is, the cohesive energies of the global minima. For $n = 13$, this analysis is in agreement with the best available theoretical results.[39] No accurate first principles results for the other magic numbers are available for comparison, but

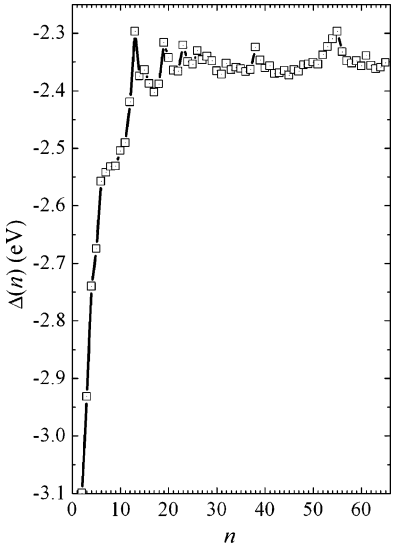

Figure 9. Excess energy function $\Delta(n)$ as a function of n. The ordinate is defined by eq 9, and for this plot, E_{coh} is taken as 3.45 eV/atom.

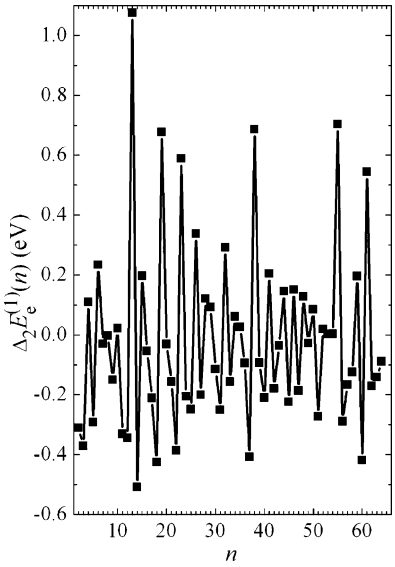

Figure 10. Second energy differences $\Delta_2 E_e^{(1)}(n)$ as a function of cluster size.

our results for the magic numbers differ from those for other analytical potentials and empirical methods such as the tight-binding method. For example, the Voter-Chen version of embedded-atom potential predicts that the magic numbers are 13, 38, 50, 54, and 61.[26] The Sutton-Chen potential predicts that the most stable clusters are $n = 4$, 6, 12, 14, 17, 21, 23, 30, 34, 39, 42, 45, 49, and 56.[29] Surprisingly, the Sutton-Chen potential predicts that Al_{13} and Al_{55} are among the most unstable particles. Chuang et al.[46] have searched the global minima of Al_n ($n = 2-23$) using a tight-binding method with a genetic algorithm. They then reoptimized the geometries of low-energy isomers using DFT method with a plane wave basis set to determine the global minima at the DFT level. They also found that 13 is a magic number. However, they concluded that 19 is not, probably because their potential is less accurate than the one used here.

However, we now recognize that an analysis of the global minima is insufficient. As cluster size increases, the energy distribution of isomers becomes almost continuous. Therefore,

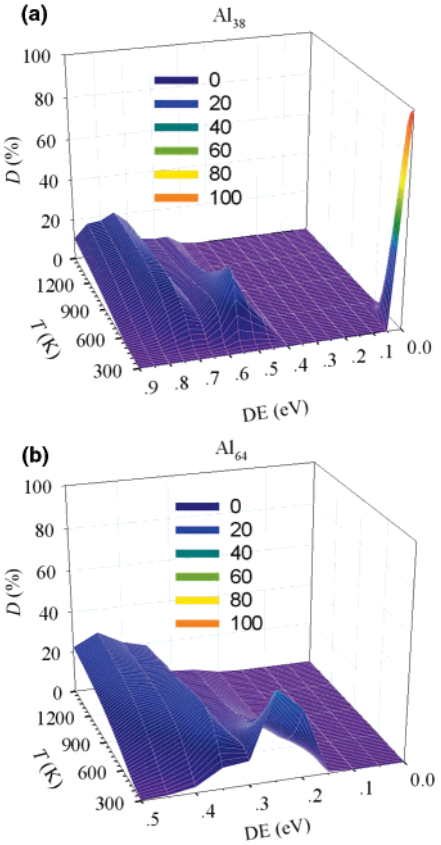

Figure 11. Three-dimensional representation of D (defined by eq 11 and calculated with $\delta E = 0.05$ eV) vs temperature T and relative energy ΔE (labeled DE in the plot) for (a) $n = 38$ and (b) $n = 64$.

one may need to look at the contributions of the isomers in a specific energy range rather than the contribution of an individual isomer. For this purpose, the probability of finding an isomer with an energy between ΔE and $\Delta E + \delta E$ is defined as

$$D = \sum_{\Delta E \leq E_e^{(\gamma)} < \Delta E + \delta E} P_\gamma \tag{11}$$

where ΔE is relative energy defined by

$$\Delta E = \Delta E_e^{(\gamma)} = E_e^{(\gamma)} - E_e^{(1)} \tag{12}$$

and δE is a resolution parameter. Plots of D vs temperature T and ΔE for selected particles, $n = 13$, 19, 23, 55, and 61 are depicted in the Supporting Information, and plots for $n = 38$ and 64 are given as Figure 11.

Figure 11a shows that the global minimum dominates at low temperature but only up to ~400 K. At higher T, the populations of the isomers at ~0.6 eV become significant but begin to decrease at ~1000 K, where isomers with $\Delta E \approx 0.7-0.9$ eV becomes prominent. Thus, Al_{38} does not have a well-ordered structure under most conditions. Al_{55} shows some similar trends. The importance of the global minimum decreases rapidly above 500 K. Al_{55} melts at ~600 K, and isomers with $\Delta E \approx 0.7-0.75$ become prominent, reaching a maximum at 700 K but constituting more than 80% of the population up to 1500 K. This strong contribution is due to the existence of 205 isomers in this energy region. Thus, the properties of the nanoparticles and the question of magic numbers (particularly stable particles, whose existence could be technologically important) can only be properly understood by a more complete statistical mechanical analysis.

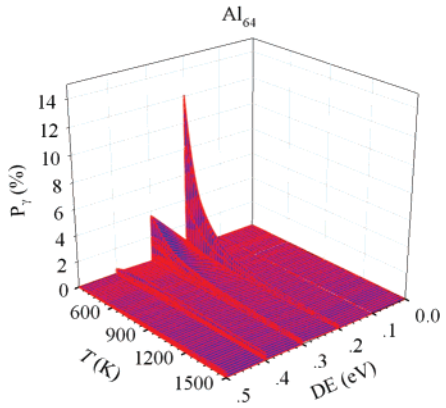

Figure 12. Probability of finding an isomer of Al_{64} as a function of temperature T. See eq 5.

Figure 12 shows P_γ vs T and ΔE for $n = 64$.

5. Statistical Nanothermodynamics

After P_γ is calculated, the correctly averaged thermodynamic properties of a particle can be calculated. For example, the thermal energy of a particle at temperature T including the electronic contribution, can be calculated by

$$\Delta E_T^{\text{tot}} = 1.5kT + E_T^{\text{Elec}} + \sum_{\gamma,v,j} (\Delta E_{\text{e}}^{(\gamma)} + \epsilon_{\gamma,v,j}) P_{\gamma,v,j} \tag{13}$$

where $1.5kT$ is the contribution from the translational motion, E_T^{Elec} is the average electronic excitation energy (assumed separable and independent of n), $\Delta E_{\text{e}}^{(\gamma)}$ is the equilibrium energy of an isomer relative to the global minimum as defined in eq 12, and $P_{\gamma,v,j}$ is

$$P_{\gamma,v,j} = \frac{e^{-(\Delta E_e^{(\gamma)} + \epsilon_{\gamma,v,j})/kT}}{Q_{\text{IsoRov}}} \tag{14}$$

where Q_{IsoRov} is the isomeric-rovibrational partition function of an particle:

$$Q_{\text{IsoRov}} = \sum_\gamma e^{-\Delta E_e^{(\gamma)}/kT} q_{\text{Rov}}^{(\gamma)} \tag{15}$$

The standard state (1 atm) Gibbs free energy of a particle is given by

$$G_{\text{T}} = E_{\text{e}}^{(1)} - kT \ln q_{\text{Elec}}\, q_{\text{Trans}}\, Q_{\text{IsoRov}} + kT \tag{16}$$

where q_{Trans} is the translational partition function. Similar to $\Delta_2 E_{\text{e}}^{(1)}(n)$, we define

$$\Delta_2 G_T(n) = G_T^{\text{tot}}(n-1) + G_T^{\text{tot}}(n+1) - 2G_T^{\text{tot}}(n) \tag{17}$$

The quantity $\Delta_2 G_T(n)$ is shown as a function of cluster size in Figure 13. At 300 K, $\Delta_2 G_T(n)$ shows trends similar to $\Delta_2 E_e^{(1)}(n)$, which does not include entropy, thermal energy, and ZPE contributions. One difference is that the prominent peak at $n = 61$ in Figure 10 vanishes already at 300 K in Figure 13. For $n = 38$, the peak in $\Delta_2 E_e^{(1)}(n)$ becomes a shallow valley in

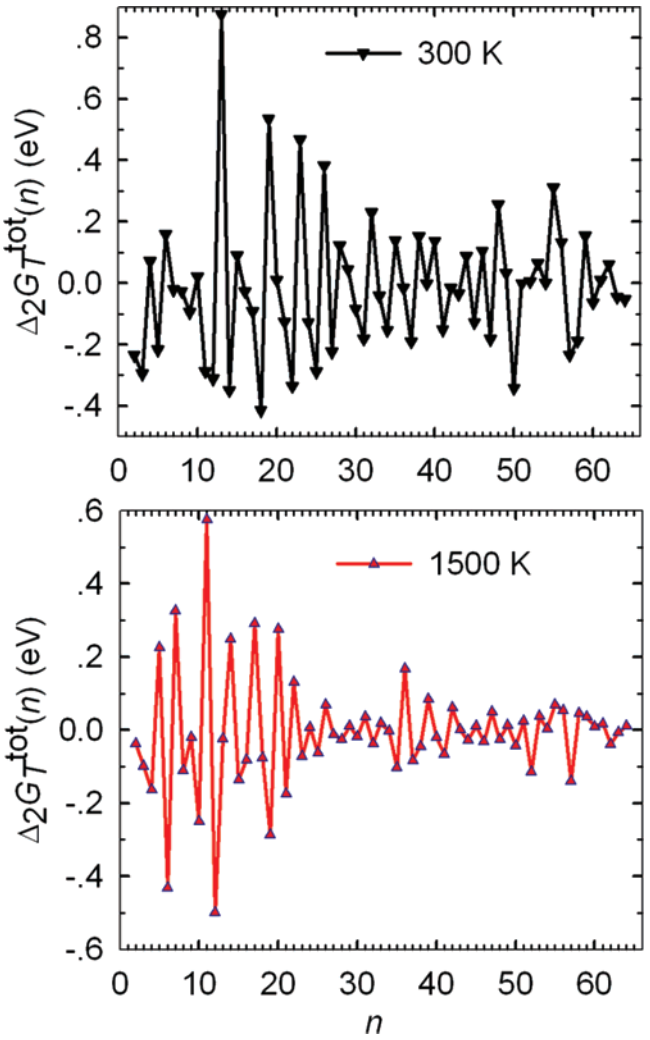

Figure 13. Second free energy difference, $\Delta_2 G_T^{tot}(n)$, as a function of cluster size. Note that ΔG_T is labeled ΔG_T^{tot} in the figure to emphasize that it includes translational, rotational, vibrational, isomeric, and electronic contributions.

$\Delta_2 G_T(n)$ by 500 K, and the valley at $n = 50$ vanishes by 800 K. The peak at $n = 55$ vanishes and shifts to $n = 56$ at 500 K, and the peak at $n = 56$ vanishes at 1500 K. Another interesting result is that at 1500 K, the high peak at $n = 19$ in Figure 10 becomes a valley in Figure 13, and a new peak at $n = 20$ appears. For other sizes, peaks frequently become valleys and vice versa on the $\Delta_2 G_T(n)$ plot, for example for $n = 5$, 7, 11, and 14.

The oscillation amplitude in $\Delta_2 G_T(n)$ plots in general decreases as temperature increases, as seen by comparing the two temperatures in Figure 13. This indicates that after a particle melts and becomes a nanodroplet, particle properties may become a smooth function of particle size. Of course, the properties of small particles (clusters) still depend greatly on particle size. The oscillation amplitude also decreases as cluster size increases so that particle properties become less dependent on size as particle sizes increases. Additional plots involving equilibrium energy, thermal energy, and free energy are given in Supporting Information. The plots, taken as a whole, show that the relative stability of metal particles is determined by additional factors beyond the commonly used cohesive energy criterion. The plots of the first and second energy differences and the first and second Gibbs free energy differences clearly indicate that the stability of a particle as a function of particle size changes with temperature; comparison of plots of the thermal energy and ZPE to plots of free energy shows some interesting differences but overall more similarity than difference, which indicates the importance of thermal energy and ZPE relative to entropy for most (but not all) trends. Knowledge of the size dependence of $\Delta_2 G_T(n)$ is useful for guiding the synthesis of nanoparticles with a desired particle size. For example, according to the $\Delta_2 G_T(n)$ plot, it may be difficult to synthesize Al_{57} particles.

Particle Isomeric Energies. With the partition functions calculated above, it is easy to calculate the average properties of an ensemble composed of a single global minimum and its surrounding basin. The thermal energy of a single isomer is

$$\Delta E_T^{(\gamma)} = 1.5kT + \Delta E_e^{(\gamma)} + E_{\text{Elec}}^{(\gamma)} + E_{\text{Rot}}^{(\gamma)} + E_{\text{Vib}}^{(\gamma)} \quad (18)$$

As before we assume $E_{\text{Elec}}^{(\gamma)}$ is independent of γ. Then we define a property that can be used to characterize the representative capability of the global minimum structure to the thermochemical properties of a particle with more than one isomer, which is the difference between ΔE_T^{tot} and the thermal energy of the global minimum, which yields

$$E_{\text{Iso}} = -(E_{\text{Vib}}^{(1)} + E_{\text{Rot}}^{(1)}) + \sum_{\gamma} (\Delta E_{\text{e}}^{(\gamma)} + E_{\text{Vib}}^{(\gamma)} + E_{\text{Rot}}^{(\gamma)})P_{\gamma} \quad (19)$$

where $E_{\text{Vib}}^{(1)}$ and $E_{\text{Rot}}^{(1)}$ are the thermal vibrational energy and thermal rotational energy of the global minimum, respectively. We name this quantity particle isomeric energy. Clearly, if E_{Iso} is close to zero, the thermochemical properties of the global minimum can well represent the properties of the particle.

Particle isomeric energy as a function of particle size is plotted in Figure 14 at four temperatures. At 300 K, for the small particles with $n \leq 30$, E_{Iso} is all close to zero. The largest E_{Iso} is at $n = 17$, where $E_{\text{Iso}} = 0.04$ eV, and the second largest E_{Iso} is at $n = 22$ and 29, where $E_{\text{Iso}} = 0.03$ eV. For $n \leq 30$, 24 of the 29 particle sizes have E_{Iso} values less than 0.02 eV. However, for $n > 30$ only 13 out of 35 particles have E_{Iso} values that are less than 0.02 eV, but eight of them have E_{Iso} values that are less than 0.01 eV. These 8 particles are Al_{35}, Al_{38}, Al_{40}, Al_{44}, Al_{48}, Al_{53}, Al_{54}, and Al_{55}. For some particles, for example for Al_{41}, Al_{50}, and Al_{61}, studying just the global minimum may cause very large error.

E_{Iso} is a monotonically increasing function of temperature. For $T = 500$ K and $n > 30$, the number of the particles with $E_{\text{Iso}} < 0.01$ eV drops to 3, in particular, Al_{48}, Al_{53}, and Al_{54}. Surprisingly, E_{Iso} of Al_{38} increases rapidly to 0.56 eV. As discussed above, this is because higher-energy isomers in a wide energy range quickly make significant contributions for Al_{38}. As temperature increases to 800 K, only 8 (including Al_2, which has only one isomer) of the 64 particles have E_{Iso}values that are less than 0.01 eV, and these particles Al_2, Al_3, Al_4, Al_6, Al_{12}, Al_{13}, Al_{19}, and Al_{56}. At 1500 K, except for Al_2, Al_3, and Al_4, all particles have large E_{Iso} values greater than 0.07 eV.

Two very interesting trends can be observed in Figure 14. The first one is that the E_{Iso} of Al_{56} does not change much from 300 to 800 K, which means in this wide temperature range, the energy of the particle can be well represented by the global minimum. However, the probability of the global minimum is very small. We have checked the structures of Al_{56}, and found that there are 53 isomers with energies no higher than 0.02 eV

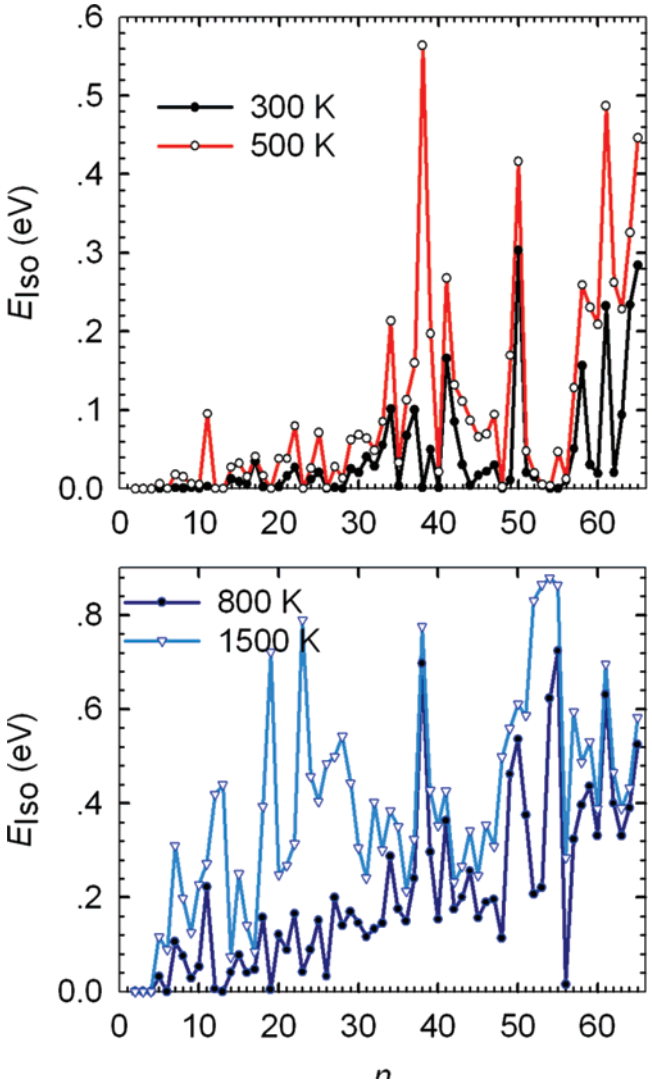

Figure 14. Particle isomeric energy (E_{Iso}, eq 19) as a function of cluster size.

above the global minimum, and two with energies just 0.07 eV higher than the global minimum. The rest are higher in energy by more than 0.41 eV. The global minimum, the second-lowest-energy isomer, and the third-lowest-energy isomer can be viewed as adsorbing an Al atom onto the isocahedral Al_{55} global minimum. The other 50 isomers can be viewed as inserting one aluminum atom into a five-member ring formed by surface aluminum atoms of the isocahedral Al_{55} global minimum to make a six-membered ring. These 53 isomers thus have very similar structures to the global minimum so that, although many structures contribute, the properties of the global minimum may still be representative. Figure 7 indicates that the low-lying 64 isomers have a total probability of more than 60% even at 1500 K (see also the Supporting Information).

For particles with $n = 12$, 13, 19, 23, 38, 52, 53, 54, and 55, the plots show a valley basin at low T changing to a peak at high T with a dramatic change in E_{Iso} values. This may correspond to a dramatic change in the particle properties that are a function of geometry (structure), and in particular it may correspond to a phase transition or a structural transition. In Figure 15, we plot the E_{Iso} values of these particles as a function of temperature. Notice that the first-order derivative of E_{Iso} with respect to temperature is the heat capacity difference between

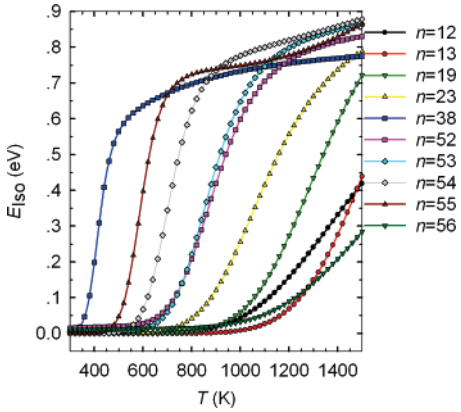

Figure 15. E_{Iso} (eq 19) as a function of temperature for particles with $n =$ 12, 13, 19, 23, 38, 52, 53, 54, 55, and 56.

the particle and the global minimum; therefore E_{Iso} can also be used to study the phase transitions or structural transition of metal particles. For example, the transition of Al_{13} begins at about 1100 K, and that of Al_{38} begins at about 350 K. It is interesting that for Al_{55}, a first transition begins at about 500 K, while there is a second transition that begins at about 1200 K; at 1200 K, high-energy isomers above 1.2 eV begin to have non-negligible probability. The isomeric energy of Al_{56} is also plotted in Figure 15 for comparison. The plot shows that Al_{56} indeed has a very late structural transition which begins at about 1000 K.

6. Conclusions

In this work, the global minimum-energy structures, as well as thousands of higher-energy local minima, have been characterized for Al_n ($2 \le n \le 65$) clusters and nanoparticles by using a combination of a big-bang random search and molecular dynamics quenching simulations. Although there has been considerable effort devoted to characterizing the minimum-energy structures of, for example, Lennard-Jonesium[7] (a system composed of atoms interacting by two-body LJ potentials), we know of no extensive systematic work employing a potential as accurate as the potential surface used here, which has been well validated for nanoparticles. Thus, even though no analytic potential is fully reliable, the structures found here can serve as starting geometries for more detailed investigations of electronic, vibrational, rotational, and reactive properties of the clusters and nanoparticles. Even more informatively, we have used them to survey (for the first time) the trends in the nanothermodynamics of a realistic model of metal particles.

Cohesive energies of the global minima and their first and second energy differences have been calculated, and, neglecting thermal energy and entropy effects, candidates for magic numbers were determined to be $n = 13$, 19, 23, 38, and 55. The thermal stability of these particles was also considered, and Al_{38} was found to lose its enhanced stability, even at modest temperatures.

The equilibrium distributions of the low-energy configurations of Al_n have been calculated for all particles up to $n = 65$, and this analysis includes the effect of the rovibrational partition functions of isomers. We find that the probability distributions of structures computed from the electronic energy alone (isomerically separable approximation) can be quite different from those computed including isomer-dependent rovibrational

free energy (isomerically coupled approximation). In general (the exceptions are $n = 4$, 5, 6, 12, and 13), the global minimum energy structure is not the dominant structure (the lowest-free-energy structure) at elevated temperatures. For some particles, it is the second-lowest-energy isomer (Al_9 and Al_{31}) or the third-lowest-energy isomer (Al_{61}) that is dominant even at room temperature. Furthermore, especially for the larger particles or at higher temperatures, so many structures contribute to the thermal distribution that it is more practical to average over structures by statistical sampling rather than by cataloging an exhaustive library of structures.

We have also analyzed in detail the equilibrium distribution of all the low-energy isomers located by the molecular dynamics quenching simulations for five candidates for magic numbered particle sizes. We found that Al_{38} may not be a magic particle since its global minimum structure is only dominant in a small temperature range above room temperature. Above 400 K, it can be viewed as a mix of many isomers in a wide energy range. Therefore, determining the magic numbers of metal particles by just considering the potential energies of the global minima is insufficient. A very interesting result obtained by analysis of the phase transition of Al_{55} is that at higher energy it is composed of similar structures in a very narrow energy range between 0.70 and 0.75 eV, which may be viewed as a quasi energy level so that the phenomenological behavior can be explained by a two-state model.

Particle isomeric energies, E_{Iso}, have been calculated to characterize the contribution of the global minimum to the properties of a particle with more than one isomer. For some particles, for example Al_{56}, even though the global minimum has a low probability even at room temperature, the properties of the particle can still be represented by the global minimum in a wide temperature range. The isomeric energy can also be used to characterize structural transitions in metal particles.

Acknowledgment. We are grateful to Nathan E. Schultz and Mark Iron for helpful discussions. This work was supported by the National Science Foundation by grant no. CHE07-04974 and by the Defense-University Research Initiative in Nanotechnology (DURINT) through a grant managed by the Army Research Office. This research was performed in part by using a Molecular Science Computing Facility Computational Grand Challenge grant at the Environmental Molecular Sciences Laboratory, supported by the United States Department of Energy at Pacific Northwest National Laboratory, operated by Battelle.

Supporting Information Available: Part 1: Additional computational details, thermodynamic equations, discussion, P_γ and C_N values, additional plots of cohesive energies and energy differences, and plots of the density of isomers vs energy. Part 2: 64 sets of Cartesian coordinates for the global minima of the Al_n ($n = 2-65$) particles in Figures 1−4. Part 3: Cartesian structures of the second-, third-, and fourth-lowest-energy minima in Figure 5. This material is available free of charge via the Internet at http://pubs.acs.org.

JA073129I